Reviews
Nanostructured, nanoscale materials and nanodevices

УДК 679.871 DOI: 10.17277/jamt-2026-11-02-172-193

Application of detonation nanodiamonds in new technologies

© Valerii Yu. Dolmatov[a]✉, Alexander A. Merkin[a], Maxim N. Kiselev[b], Nataliya P. Satonkina[c], Natalia M. Lapchuk[d], Anna N. Oleshkevich[d], Kristina V. Lotnikova[a], Vladimir T. Senyut[e], Sergey D. Pisarevsky[f], Alla V. Nozhkina[g], Alexander P. Ershov[c]

[a] *Special Design and Technology Bureau "Tekhnolog", 33-a, Sovetsky Av., St. Petersburg, 192076, Russian Federation,*
[b] *JSC "Plant "Selmash", 66, Shchorsa St., Kirov, 610014, Russian Federation,*
[c] *Lavrentiev Institute of Hydrodynamics of Siberian Branch of RAS, 15, Lavrentieva Av., Novosibirsk, 630090, Russian Federation,*
[d] *Belarusian State University, 4, Nezavisimosti Av., Minsk, 220030, Belarus,*
[e] *The Joint Institute of Mechanical Engineering of the NAS of Belarus, 12, Akademicheskaya St., Minsk, 220072, Belarus,*
[f] *Geoinformation Systems of the NAS of Belarus, 6, Surganova St., Minsk, 220012, Belarus,*
[g] *JSC "Research Institute of Natural, Synthetic Diamonds and Tools", 65, Gilyarovsky St., Moscow, 107996, Russian Federation*

✉ diamondcentre@mail.ru

Abstract. This review summarizes the results of using detonation nanodiamonds (DNDs) over the past 10 years in emerging areas of science and technology. Oriented coalescence of nanodiamond crystallites (~ 4 nm) under high temperature and pressure leads to the formation of single crystals with multi-micron dimensions. New magnetic resonance imaging contrast agents have been proposed and studied in the form of aqueous suspensions containing DNDs doped with manganese and gadolinium ions. The potential use of DND crystallites as reflectors for very slow neutrons (~ 50 $m \cdot s^{-1}$) has been demonstrated. The feasibility of producing diamond coatings containing europium ions by the CVD-method has been shown. An electrorheological effect was observed when an electric field is applied to suspensions of nanodiamond crystallites in oils, with DND crystallites acting as nodes in a fractal conductive network. Mixing DNDs with tungsten (W) powder followed by sintering increases the Young's modulus of sintered tungsten by a factor of four and its hardness by 1.5–2.0 times. Replacing standard DNDs (derived from TNT/RDX mixtures) with boron-doped DNDs produced during detonation synthesis further increases the microhardness of sintered tungsten by up to four times. New types of pseud alloys were obtained for the first time: an aluminum-tungsten alloy containing 10 wt. % tungsten and 90 wt. % aluminum with a hardness of HB 60, and an aluminum-copper-tungsten alloy containing 15 wt. % Al, 50 wt. % Cu, 35 wt. % W, and 1.2 wt. % DNDs. The resulting compositions are readily machinable. The use of aqueous nanodiamond suspensions in photonics has been demonstrated for producing linear optical filters resistant to high-power radiation. Application of an intermediate product from DND synthesis – diamond charge – increased the germination rate of Chinese cabbage seeds by 70 % compared to normal rates. Adding diamond charge to space-grade lubricants reduced component wear by a factor of two. Modification of paste-like fuels with nanodiamonds increased their burning rate by up to 23%.

Keywords: detonation nanodiamonds; sintering; modification; electroplating; slow neutron reflectors; tungsten-containing alloys; fuel; space lubricants.

For citation: Dolmatov VYu, Merkin AA, Kiselev MN, Satonkina NP, Lapchuk NM, Oleshkevich AN, Lotnikova KV, Senyut VT, Pisarevsky SD, Nozhkina AV, Ershov AP. Application of detonation nanodiamonds in new technologies. *Journal of Advanced Materials and Technologies*. 2026;11(2):172-193. DOI: 10.17277/jamt-2026-11-02-172-193

Применение детонационных наноалмазов в новых технологиях

© В. Ю. Долматов[a]✉, А. А. Меркин[a], М. Н. Киселев[b], Н. П. Сатонкина[c], Н. М. Лапчук [d], А. Н. Олешкевич[d], К. В. Лотникова [a], В. Т. Сенють[e], С. Д. Писаревский[f], А. В. Ножкина[g], А. П. Ершов[c]

[a] *Специальное конструкторско-технологическое бюро «Технолог», Советский пр., 33-а, Санкт-Петербург, 192076, Российская Федерация,*
[b] *АО «Завод «Сельмаш», ул. Щорса, 66, Киров, 610014, Российская Федерация,*
[c] *Институт гидродинамики им. М. А. Лаврентьева СО РАН, пр. Лаврентьева, 15, Новосибирск, 630090, Российская Федерация,*
[d] *Белорусский государственный университет, пр. Независимости, 4, Минск, 220030, Республика Беларусь,*
[e] *Объединенный институт машиностроения НАН Беларуси, ул. Академическая, 12, Минск, 220072, Республика Беларусь,*
[f] *УП «Геоинформационные системы» НАН Беларуси, ул. Сурганова, 6, Минск, 220012, Республика Беларусь,*
[g] *ОАО «Научно-исследовательский институт природных, синтетических алмазов и инструмента», ул. Гиляровского, 65, Москва, 107996, Российская Федерация*

✉ diamondcentre@mail.ru

Аннотация. Обзор обобщает результаты использования детонационных наноалмазов (ДНА) за последние 10 лет для новых областей науки и техники. Ориентированное сращивание кристаллитов наноалмазов (~ 4 нм) при воздействии высоких температур и давлении способствует образованию монокристаллов многомикронных размеров. Предложены и изучены новые контрастные МРТ-вещества в виде водных суспензий с введенными в них ДНА, легированные ионами марганца и гадолиния. Показана возможность использования кристаллитов ДНА в качестве отражателей очень медленных нейтронов (~ 50 м/с). Показана возможность получения (CVD-метод) алмазных покрытий, содержащих ионы европия. Обнаружен электрореологический эффект при наложении электрического поля на суспензию кристаллитов наноалмазов в маслах, причем кристаллиты ДНА являются центром узлов фрактальной токопроводящей сетки. Смешивание ДНА с порошком вольфрама (W) при последующем спекании приводит к усилению модуля Юнга в 4 раза и твердость в 1,5–2,0 раза у спеченного W. Замена стандартных ДНА (из смеси тротила с гексогеном) на ДНА, легированных бором при детонационном синтезе, увеличивает микротвердость спеченного W дополнительно до четырех раз. Впервые получены новые виды псевдосплавов – алюмовольфрамовый, содержащий 10 мас. % вольфрама и 90 мас. % алюминия с твердостью НВ 60 и алюминиево-медно-вольфрамовый, содержащий 15 мас. % Al, 50 мас. % медь, 35 мас. % вольфрам и 1,2 мас. % ДНА. Полученные составы легко подвергаются механической обработке. Показана возможность использования водных суспензий наноалмазов в фотонике с целью получения линейно-оптических фильтров, устойчивых к мощному излучению. Применение полупродукта синтеза ДНА-алмазной шихты (АШ) привело к увеличению всхожести семян пекинской капусты на 70 % по сравнению с обычной всхожестью таких семян. Введение АШ в используемые космические смазки снизило износ деталей в 2 раза. Модификация пастообразных топлив наноалмазами позволила поднять скорость их горения до 23 %.

Ключевые слова: детонационные наноалмазы; спекание; модифицирование; гальваника; отражатели медленных нейтронов; вольфрамсодержащие сплавы; топливо; космические смазки.

Для цитирования: Dolmatov VYu, Merkin AA, Kiselev MN, Satonkina NP, Lapchuk NM, Oleshkevich AN, Lotnikova KV, Senyut VT, Pisarevsky SD, Nozhkina AV, Ershov AP. Application of detonation nanodiamonds in new technologies. *Journal of Advanced Materials and Technologies*. 2026;11(2):172-193. DOI: 10.17277/jamt-2026-11-02-172-193

List of Abbreviations

BTF – benzotrifuroxan (benzotris);
CEC – composite electrochemical coating;
CJ plane – Chapman–Jouguet plane;
CRZ – chemical reaction zone during explosive decomposition of HE;
DC – diamond detonation charge;
DND – detonation nanodiamond;
DP – detonation products;
EPR – electron paramagnetic resonance;
FL – fluorescence;
HE – high explosive;
HPHT – a widely used method for layer-by-layer diamond film growth at high temperatures and pressures;
MRI – magnetic resonance imaging;

NMR – nuclear magnetic resonance;
NV – nitrogen-vacancy center;
OB – oxygen balance of the explosive;
PA – picric acid;
PVP – poly(N-vinylpyrrolidone);
RDX – cyclotrimethylenetrinitramine (hexogen);
SEM – scanning electron microscopy;
TATB – 1,3,5-triamino-2,4,6-trinitrobenzene;
TEM – transmission electron microscopy;
TG – charge composed of TNT and RDX;
TNT – 2,4,6-trinitrotoluene.

1. Introduction

Detonation (ultradispersed) nanodiamonds (DNDs) were discovered by Russian scientists in 1963 [1]. Their synthesis uses carbon-containing high explosives (HEs) that have an insufficient amount of oxidizer (oxygen) in their molecular structure. As a result, only part of the carbon is oxidized into gaseous products, while the remaining carbon is released in solid form within the detonation products (DP). Under certain conditions (defined by 12 key control parameters), DNDs form and persist within these solid carbon products [2–5].

The resulting DNDs have a complex structure: inside each crystallite (~5 nm) there is a classical diamond cubic lattice, but closer to the surface the crystal structure gradually transforms – from "diamond-like" sp^3-hybridization to "graphite-like" sp^2-hybridization of carbon with each coordination shell [6]. The surface of DND particles predominantly contains oxygen-containing functional groups such as hydroxyl, carbonyl, carboxyl, ester groups, etc. [3].

Typically, nanodiamonds are produced using a mixture of TNT and RDX in proportions ranging from 60/40 to 40/60 [1, 3].

At present, there is a significant resurgence of interest in DNDs. New types of high explosives (HEs), including those derived from decommissioned materials, are being used. Research is underway on producing doped (modified) DNDs, improving various methods of nanodiamond functionalization, and developing relatively simple and environmentally acceptable purification technologies. Doping DNDs with silver, gold, and platinum opens up the possibility of creating superconducting materials in the near future and expands their potential applications in micro- and nanoelectronics. Achieving high concentrations of NV centers in nanodiamond crystallites contributes to the development of nanodiamond-based spintronics.

Industrial production (in Russia, Belarus, China, and Japan) is based on the use of mixtures of TNT (2,4,6-trinitrotoluene) and RDX (cyclotrimethylenetrinitramine). In Russia, a technology based on tetryl (N-methyl-N-2,4,6-tetranitroaniline) has also been developed. These explosives serve simultaneously as both an energy source and a carbon source. The use of DNDs across various industries is driven by the need to significantly improve the performance characteristics of composite materials.

The cost of DNDs is relatively affordable, industrial-scale production exists, and market expansion is expected. However, DNDs cannot yet be considered a fully well-characterized diamond material. This is due to variability in surface chemical composition, crystal structure, and therefore properties, which depend on differences in synthesis and purification technologies among manufacturers [1–5].

The aim of this review is to systematize empirical and theoretical knowledge on the application of detonation nanodiamonds in various fields of science and technology.

2. Oriented sintering of DNDs

Under high temperature (1300–1800 °C) and pressure of 5–7 GPa (~ 50,000–70,000 atm.), DNDs introduced into mono- or dihydric alcohols form single-crystal diamonds up to 50 μm in size with a highly perfect crystal structure [7].

Most likely, according to the theory of A. Barnard [8], at high temperatures nanodiamonds – temporarily existing as individual crystallites in liquid alcohols – become oriented relative to one another through oppositely charged crystal facets and "collapse" together in accordance with Coulomb's law. It is also possible that the carbon-containing alcohols, upon further decomposition at high temperature, act as an additional carbon source, which under high pressure becomes incorporated into the newly forming crystal structure of micron-sized diamonds.

Since the resulting diamonds are multi-micron in size and exhibit a highly perfect crystal structure, reconstruction also occurs in the carbon atoms of the defective near-surface regions of each DND crystallite. In addition, carbon generated from alcohol decomposition likely fills microdefects formed during oriented sintering due to the imperfect shape of the initial nanodiamond particles.

Prior to sintering, isopropyl or ethyl alcohol, ethylene glycol, glycerol, and other alcohols were added to DND powder. The influence of alcohol content in the range of 5–60 wt. % was investigated.

The yield of micron-sized diamond crystals from the initial DND mass was significant – up to 100 %. The resulting particle size range was broad, from 70 nm to 15 μm, with the majority consisting of microdiamond particles ≥ 4 μm.

As seen in Fig. 1, the authors [7] obtained faceted single-crystal diamonds during sintering, with sizes reaching up to 15 μm (average size ~ 1 μm). Figure 1a shows that a significant portion of microcrystals exhibit an octahedral shape.

Raman spectroscopy confirms the single-crystal nature of the sintered DNDs. The resulting product shows only a single narrow symmetric peak at 1332 cm^{-1}, corresponding to the diamond crystal lattice.

Further evidence of the high structural perfection of the obtained crystals is that the full width at half maximum (FWHM) of the 1332.3 cm^{-1} band is 2.9 cm^{-1}, compared to 3.0 cm^{-1} for natural diamond. The growth of defect-free microdiamonds from defective nanodiamond precursors most likely proceeds via an oriented attachment mechanism, which is only possible for particles with a truncated octahedral shape. This geometry enables the formation of void-free crystals.

In addition, it was established that the formation of high-quality microcrystals from defective nanocrystallites is only possible when a saturated acyclic hydrocarbon is added to the DNDs. No difference was observed between the sintering of agglomerated and deagglomerated nanodiamonds (Fig. 2).

In these micron-sized nanocrystals, an ensemble of point defects (in particular, NV centers) forms without the need for irradiation by high-energy particles.

3. Nanodiamonds functionalized with Gd and coated with PVP as a new and potentially safer MRI contrast agent

The aim of study [10] was to investigate the feasibility of using a saline suspension of DNDs coated with polyvinylpyrrolidone (PVP) and functionalized with gadolinium (Gd) as a new MRI contrast agent.

Stable saline suspensions of highly purified, deagglomerated Gd-functionalized DND particles coated with a protective PVP shell were prepared. Proton relaxivities T1 and T2 of suspensions with different gadolinium concentrations were measured at 8 Tesla. A series of *ex vivo* (phantom) and *in vivo* dynamic scans were obtained using 3 Tesla MRI, comparing PVP-coated Gd-functionalized DNDs with gadoterate meglumine at equal gadolinium concentrations. T1-weighted hyperintensity was then evaluated.

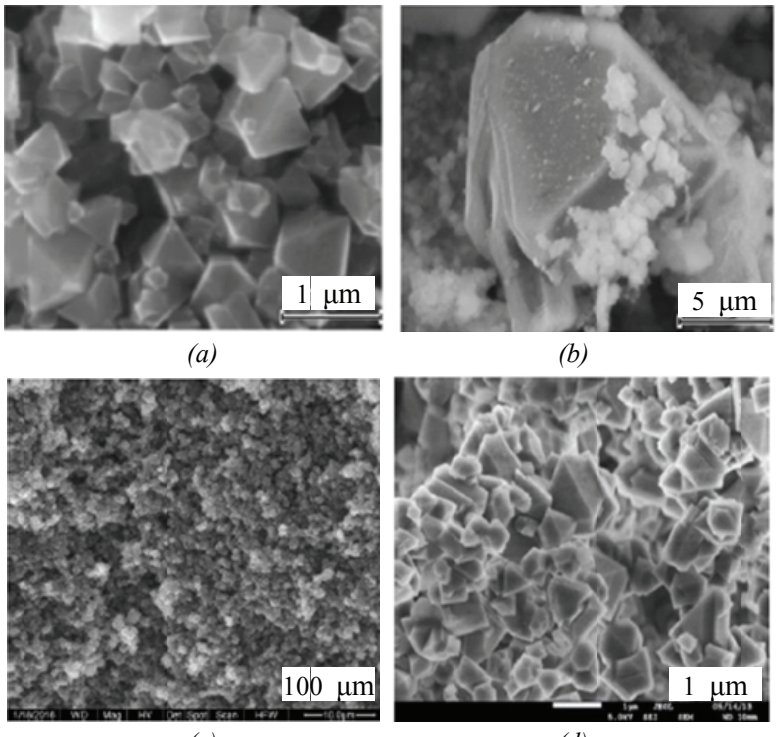

(a) *(b)* *(c)* *(d)*

Fig. 1. Appearance of oriented-sintered diamonds (scanning electron microscopy): *a* – scale 1 μm; *b* – scale 5 μm; *c* – scale 10 μm; *d* – scale 100 μm [7]

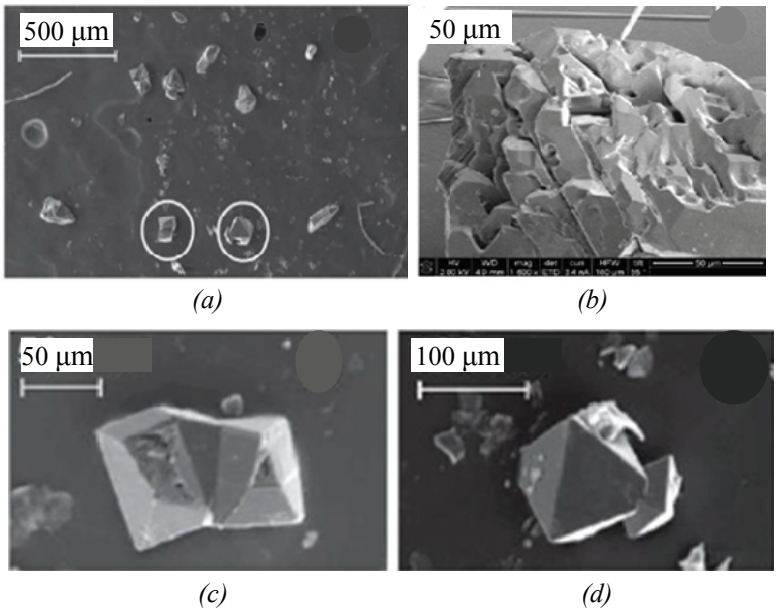

Fig. 2. *a* – Appearance of diamond single crystals after oriented attachment; *b* – surface morphology of a diamond crystal corresponding to the oriented attachment mechanism (scale 50 μm), scanning electron microscopy; *c*, *d* – obtained diamond single crystals (~100 μm) [9]

It was found that the proton relaxivity coefficients for PVP-coated Gd-functionalized DNDs were $r_1 = (33.4 \pm 0.8)$ $s^{-1} \cdot mM^{-1}$ and $r_2 =$ $= (332 \pm 15)$ $s^{-1} \cdot mM^{-1}$ [10], respectively. These values are slightly lower than those for uncoated Gd-functionalized DNDs, but still remain relatively high. MRI evaluation *ex vivo* demonstrated dose-dependent T1-weighted hyperintensity, with a significant advantage over gadoterate meglumine. Similar results were observed in *in vivo* testing of the two contrast agents.

Thus, the new MRI contrast agent-saline suspensions of PVP-coated Gd-functionalized DNDs – provides significantly higher signal intensity than the conventional agent gadoterate meglumine, increasing its potential for safer clinical use.

4. Manganese-functionalized detonation nanodiamonds as a new potential MRI contrast agent

In an effort to develop universal MRI contrast agents, the authors [11] report the synthesis and magnetic resonance study of DNDs with manganese ions directly grafted onto their surface. The sample was obtained by reacting an aqueous suspension of nanodiamonds with an aqueous solution of manganese sulfate. Evidence is presented for the chemical bonding of Mn^{2+} ions to the nanodiamond surface; these ions interact with the electronic and nuclear spins of the diamond nanoparticle, thereby accelerating spin-lattice relaxation. The distance between the Mn^{2+} ion and the diamond surface was estimated using ^{13}C NMR relaxation data. Comparison of Mn-DND interactions with previously studied Gd-functionalized DNDs [10] suggests that Mn-NDs may serve as promising MRI contrast agents.

Thus, highly purified nanodiamond particles with surfaces functionalized by paramagnetic manganese ions were obtained for the first time. The Mn grafting was achieved via ion exchange, where Mn^{2+} ions replaced hydrogen atoms of carboxyl groups during the reaction between an aqueous DND suspension and a manganese sulfate solution. NMR and EPR studies provide clear evidence that Mn^{2+} ions are chemically bound to the DND surface and interact with the electronic and nuclear spins of the diamond nanoparticles, leading to accelerated nuclear spin-lattice relaxation. The distance between Mn^{2+} ions and the DND surface, estimated from ^{13}C relaxation data, lies in the range of 0.25–0.36 nm. The authors showed that manganese functionalization reduces the ^{13}C spin-lattice relaxation time $Tln(^{13}C)$, with values comparable to those observed for Gd^{3+}-functionalized DNDs. They suggest [12] that Mn-functionalized nanodiamonds could be promising candidates for MRI contrast agents. Their safety and effectiveness will require further investigation, similar to studies conducted for Gd-functionalized DND suspensions [10].

In study [13], a new approach is reported that enables determination of spatially resolved nuclear spin–lattice relaxation times and NMR linewidths in nanomaterials. This method was applied to DNDs with manganese ions directly grafted onto their surface [11]. Interaction between carbon nuclear spins and paramagnetic Mn^{2+} ions leads to accelerated spin-lattice relaxation and broadening of the ^{13}C resonance line. Using spin dephasing experiments, the authors were able to determine the layer-by-layer contribution of Mn^{2+} ions to relaxation times and linewidths of carbon spins located at different depths from the diamond surface.

Although developed for nanodiamonds, this approach is more general and can be successfully applied to study distributions of nuclear relaxation rates and linewidth broadening, as well as to map magnetic interactions within various nanoparticles. This has practical applications in multiple nanotechnology fields. In particular, it enables investigation and tuning of magnetic interactions in DND particles functionalized with paramagnetic ions. The resulting insights are relevant for applications in spintronics, memory devices, magnetic data storage, sensors, and for studying the influence of paramagnetic ions on the relaxation of NV centers in diamonds.

5. Effect of particle size of fluorinated nanodiamonds on the efficiency of neutron reflectors

More than ten years ago, it was demonstrated that DND powders diffusely reflect very cold neutrons (VCNs) at any angle of incidence and reflect cold neutrons quasi-specularly at small angles of incidence [14]. This study investigated the neutron reflection efficiency of nanodiamonds as a function of their size. To do so, a fraction of smaller DND nanoparticles (referred to here as S-DNDs) was separated from the initially broad size distribution by centrifugation. The neutron reflector performance of these particles was then compared, both experimentally and theoretically, with that of deagglomerated fluorinated DNDs (DF-DNDs).

Typical commercially available DNDs with a size of ~ 4.3 nm are close to optimal for VCNs with a typical velocity of ~ 50 $m \cdot s^{-1}$. Smaller DNDs are more efficient for higher neutron velocities, while larger ones are more effective for slower VCNs.

Neutrons serve as both tools and subjects in many areas of research. Major global efforts are focused on increasing the intensity of neutron sources and improving neutron delivery efficiency for experimental facilities. In this context, neutron reflectors play a key role, as they can significantly enhance both efficiency and cost-effectiveness. For slow neutrons, DND powders exhibit exceptionally strong reflective properties due to a combination of enhanced coherent scattering and low neutron absorption.

The enhancement is maximized when the nanoparticle diameter is close to the neutron wavelength. Therefore, both the average particle size and the size distribution are critical factors. Additionally, DNDs tend to form clusters, which effectively increases their particle size. Study [14] reports on how the breakup of agglomerates influences DND clustering and overall reflector performance.

The authors [14] characterized DNDs using small-angle neutron scattering, X-ray diffraction, scanning and transmission electron microscopy, neutron activation analysis, dynamic light scattering, infrared spectroscopy, and other methods. Based on these results, they discuss the calculated particle size distribution of DNDs, absolute neutron scattering cross-sections, neutron albedo, and the neutron intensity gain coefficient for neutron traps with DND-based walls.

Fluorination of DNDs has little effect on the nanoparticle size distribution or the surface chemical composition.

Reducing the size of DND clusters increases neutron albedo and neutron storage time, especially in closed nanodiamond-based traps.

5. Eu-doped nanocrystalline diamond films (CVD)

Paper [15] presents experimental results on the formation of luminescent centers of europium ions in CVD diamond films. The new approach is based on using nanodiamond particles with surfaces modified by Eu ions as seed material for CVD growth. Europium-doped nanocrystalline diamond (NCD) films were grown from the gas phase on silicon substrates using microwave plasma CVD at a frequency of 2.45 GHz. Photoluminescence spectra clearly show several electronic transitions of Eu^{3+} ions, confirming their incorporation into the NCD film.

In study [15], DND particles functionalized with Eu^{3+} ions (DND–COO–{Eu}) were used to synthesize a europium-containing NCD layer. Eu-containing DND particles were attached to a 300 nm thick NCD film grown by CVD through ultrasonic treatment. Subsequent overgrowth of the

NCD film resulted in the formation of a europium-containing diamond layer. The europium ions were not etched away from the surface and remained embedded in the film. Photoluminescence analysis clearly revealed multiple electronic transitions of Eu^{3+} ions, confirming their incorporation into the NCD structure. Thus, by combining CVD growth with Eu^{3+}-functionalized DND particles, luminescent europium centers were successfully created in NCD films.

6. Electrorheological fluids with detonation nanodiamonds

Study [16] investigated the feasibility of using oils (mineral, olive, and silicone) filled with DND crystallites as electrorheological fluids. The introduced deagglomerated nanodiamonds were characterized by specific surface chemical groups, faceted shapes, and a narrow size distribution (2–10 nm, with the majority in the 3–7 nm range). The authors [16] used DND crystallites with sizes of 4 and 5 nm.

The resulting sols exhibited high sedimentation stability. An increase in viscosity was observed with increasing nanodiamond concentration, along with the emergence of a yield stress even at low nanoparticle concentrations.

A fractal structure formed by DND particles was proposed and confirmed by cryogenic tomography [16]. This method revealed differences in the fractal structure of sols depending on the type and quantity of functional groups on the nanodiamond surface. In particular, fractals formed by carboxylated DNDs are more compact than those formed by hydrogenated nanodiamonds (where a percolation network is formed, with a DND concentration of about 1 wt. %). In carboxylated nanodiamonds, the charge is localized near the functional groups.

For both hydrogenated and carboxylated nanodiamonds, the interactions between DND particles are governed by a balance between Coulomb forces and van der Waals forces. The observed differences in particle interaction depend on the nature of the liquid, particularly the dielectric properties of the solvent.

Particle size has a greater influence on the sedimentation stability of the sol than the nature of the solvent. For example, in hydrogenated DNDs, the sedimentation ratio is higher for suspensions with 5 nm particles than for those with 3 nm particles (0.95 and 0.74, respectively).

This difference in sedimentation stability may be attributed to variations in particle surface area and less pronounced charge distribution on the facets of 3 nm DND particles. These smaller particles exhibit less well-defined faceting and a higher density of structural defects.

Regardless of the type of oil used, sols of hydrogenated DNDs exhibit an electrorheological effect when an electric field is applied, whereas sols containing carboxylated nanodiamonds show electrophoresis. Thus, the nature of surface functional groups plays a decisive role in determining the behavior of DND suspensions under an electric field.

Small-angle X-ray scattering results demonstrate that 5 nm DND crystallites form significantly more branched, three-dimensional fractal structures, providing a greater number of conductive pathways in sols compared to similar structures formed by 3 nm particles. A portion of the smaller particles does not participate in fractal structure formation and remains isolated.

Carboxylation of the DND surface promotes electrophoretic motion of nanodiamond crystallites under an applied electric field in dielectric solvents. This is due to the dissociation of carboxyl groups facilitated by layers of adsorbed water on the DND surface, which generate surface charges upon dissociation.

7. Electroplating

The development of technologies for applying DND in electroplating has required further optimization both in terms of the quality of the resulting coatings and the quality and quantity of the diamond component used [3, 17]. In essence, solving this problem remained at the level of the 1980s in Russia, China, South Korea, India, Belarus, Finland, and other countries.

A striking and attractive feature of DND is the narrow range of crystal core sizes of the particles (4–5 nm). After chemical purification and removal of non-diamond (graphite-graphene) carbon-which partially hinders full aggregation of DND crystallites-agglomeration intensifies, and the size of DND agglomerates produced by industrial synthesis ranges from hundreds of nanometers to several microns.

The problem of agglomeration in dried DND powders is even worse: agglomerates range in size from single microns to tens of microns. Such particles are unsuitable for electroplating processes, as they lead to a deterioration of coating properties. However, even the use of ~ 4 nm DND nanoparticles obtained by the complex and expensive method of the Ioffe Institute does not provide any advantages over the use of DND-TAN produced by the method of the

FSUE "SKTB "Technolog," [18]. Empirically, it was established that for electroplating processes the optimal agglomerate size is 30–70 nm, which are essentially the first non-destructible agglomerates.

The solution to the problem lies in the ability to control the structure and its transformation during the creation of a new type of powder compositions based on DND, capable of disintegration in an aqueous medium into nanosized particles, and their effective use in the process of applying electrochemical metal–diamond coatings [18, 19].

To date, DND can be used for electroplating in the form of aqueous suspensions obtained immediately after chemical purification of the explosion intermediate product – ASh. After detonation of the explosive material, nanodiamond particles of various sizes are formed: crystallites of 3 to 8 nm dominate, a smaller amount in the range of 10 to 18 nm is present, and some individual particles in the range of 20 to 40 nm are also formed. The ratio of these groups strongly depends on the type of explosive and the parameters of detonation synthesis. However, due to the charge heterogeneity of the faces of a single DND particle, Coulomb interactions cause them to combine into aggregates: primary aggregates range from 10 to 50 nm (the most difficult to break down), secondary aggregates range from 70 to 250 nm, and tertiary aggregates range from 250 nm to several microns (the easiest to disintegrate). Even strong ultrasonic or mechanical disintegration cannot destroy primary aggregates and only weakly affects secondary ones.

In addition, partially disintegrated DND in suspension in strong electrolytes re-agglomerate due to the formation of multiple ion layers from the electrolyte on the surface of DND particles and their aggregates, which promotes further aggregation into rather "loose" structures that hinder the deposition of high-quality metal-diamond coatings. As a result, it becomes necessary to transport a relatively inefficient 5 % DND suspension over long distances (at higher concentrations the suspension becomes difficult to flow), meaning that 1 part of DND corresponds to approximately 20 parts of aqueous "ballast." Furthermore, such a suspension is sensitive to freezing, since this leads to irreversible agglomeration of DND particles.

It is necessary to develop dry compositions (DC) that are stable during long-term storage without changes in their properties and effective when used in aqueous solutions of strong electrolytes for the deposition of electrochemical and chemical metal-diamond coatings (chromium, nickel, copper, silver, gold).

This problem has been solved as follows: the native DND suspension obtained after chemical purification is treated with an aqueous solution of a surfactant (SAS) under simultaneous strong energy input (ultrasound, mechanical activation in a disintegrator, etc.). The surfactant penetrates the aggregated DND through macro-, micro-, and nanopores and adsorbs onto the surface of DND particles and their aggregates due to adsorption and van der Waals forces, as well as through compensation (neutralization) of electrical charges.

Next, an alkaline agent containing a carbonyl group is introduced into the suspension, and the suspension is again subjected to high-energy treatment, facilitating the penetration of metal or non-metal carbonates as deeply as possible into the DND aggregates. After this, the aqueous suspension of the primary composite is dried, crushed, and a calculated amount of dry acid (for example, citric acid) is added. The material is again ground and mixed, producing the final composite suitable for introduction into an aqueous electrolyte solution for the formation of metal–diamond coatings [19].

When the dry composite is introduced into water, soluble salts and the acid dissolve, and the carbonates react with the acid, releasing carbon dioxide gas, which disrupts the DND aggregates. The presence of the surfactant in the solution prevents re-agglomeration of the disaggregated DND particles and their primary aggregates.

In addition, due to the high disaggregation of DND and the activation of their surface, an increase in their activity is expected, along with the possibility of reducing their loading in electroplating baths. For example, if standard chromium plating requires a DND concentration of 10–15 $g \cdot L^{-1}$, the proposed product requires only 5 $g \cdot L^{-1}$, with an operating concentration range from 5 down to 1 $g \cdot L^{-1}$.

Thus, preliminary testing of various DND-containing compositions obtained under different conditions has so far identified only one formulation out of 17 that met the required quality criteria for wear-resistant chromium–diamond coatings (an increase in wear resistance of up to 4 times) at a DND concentration of 5.0 $g \cdot L^{-1}$ (Table 1). It is clear that reducing the DND loading in the electroplating bath by a factor of 2–3 significantly improves the economics of the process, especially at the initial, most cost-intensive stage.

Table 1. Comparative values of microhardness and wear resistance (wear-resistant chromium): Cr_3O – 250 g·L^{-1}, H_2SO_4 – 2.5 g·L^{-1}, SC (in terms of DND) – 5.0 g·L^{-1}. Deposition regime: current density – 50 A·dm^{-2}, electrolyte temperature – 55 °C. DND concentration – from 5.0 to 1.0 g·L^{-1} in the electrolyte [19]

Amount of additive calculated based on DND, g·L^{-1}	Microhardness H_μ, kgf·mm^{-2}. Coating thickness: 20 μm (40 min)							Wear, g
	Point 1 (center)	Point 1 (center)	Point 3 (top left)	Point 4 (bottom right)	Point 5 (bottom left)	Average	Difference between maximum and minimum values	
–	690	750	887	874	892	818	202	0.043
5.0	1050	1032	982	994	1057	1023	75	0.011

It is relevant to develop a universal diamond-containing dry powder capable of ensuring high-quality deposited coatings (chromium, nickel, copper, silver, gold) at low electrolyte concentrations. Such a powder should have a long shelf life (at least 5 years) without deterioration of properties, be resistant to freezing, be easily introduced into the electrolyte, and provide a wide range of working concentrations relative to the initially introduced amount (up to 80 %).

It should be noted that achieving a microhardness above 1050 kg/mm² for wear-resistant chromium leads to negative consequences – reduced wear resistance due to embrittlement and crack formation (numerous fine cracks appear), as well as decreased adhesion of the chromium-nanodiamond coating to the substrate surface.

In [20], the authors used a sulfuric acid electrolyte and an intermediate product (ASh) obtained from the detonation of a TNT–RDX mixture, containing 56 % DND, to produce an anodic coating. Under test conditions, the oxide layer containing ASh does not wear off. After 220 hours of exposure in a climate chamber, no signs of corrosion were detected on samples with ASh, whereas without ASh, corrosion traces appeared after 96 hours.

In this paper, for the first time, the influence of ASh on the anodizing process in a sulfate electrolyte was studied with the aim of eliminating the impregnation step from the technological chain. At an ASh concentration of 2 g·L^{-1}, a high microhardness of the oxide coating is achieved – up to 10 GPa·mm^{-2}. The corrosion resistance of the oxide layer obtained in an electrolyte with 3 g·L^{-1} ASh is at least 2.4 times higher than that of films produced under standard conditions with water impregnation. The porosity of films obtained in an electrolyte with 3 g·L^{-1} ASh is 2.5 times lower than that of films produced under standard conditions.

For obtaining anodized aluminum or aluminum alloy coatings with high performance characteristics, the following electrolyte composition is recommended:

– sulfuric acid – 200 g·L^{-1};
– diamond-containing charge – 2.0–3.0 g·L^{-1};
– remainder – water;
– process temperature – not higher than +12 °C.

8. Tungsten alloys with DND

Tungsten (W) has many unique properties, including resistance to very high temperatures, high density and hardness, and excellent wear resistance, which determine its use in tool manufacturing, mechanical engineering, and the aerospace industry. It has the highest melting point (3420 °C) and high thermal conductivity [21, 22]. A disadvantage of tungsten is its high brittleness. However, reducing the grain size of the powder improves ductility, machinability of tungsten compacts, and resistance to chipping [23]. In addition, the authors of [24–27] suppress possible grain growth of W at high temperatures by adding ultrafine particles such as ZrC, HfC, La_2O_3, Y_2O_3, CeO_2, or TiC.

In studies [25], fullerene C_{60} and DND were used as nanoscale carbon additives to tungsten, with primary sizes of a single molecule and 4–6 nm particles, respectively.

The sample preparation scheme consisted of four stages:

1) milling of the initial powders to a size of ≤ 50 nm;

Table 2. Parameters of sintered tungsten-containing samples [25]

Composition, wt. %	*P*, GPa	*T*, °C	OCR before sintering, nm	ρ, g·cm^{-3}	OCR after sintering, nm	Microhardness (Vickers), GPa	*E* (Young's modulus), GPa
W 100 %	5.3	1220	34	18.4	37–38	7.7	290
		1380	34	18.5	46–47	7.2	285
		1550	34	18.4	47–48	6	283
		1700	34	18.6	48–50	5.3	278
W 99.7 % – nanodiamond 0.3 %	5.3	1220	34	18.2	30	13.0	895
		1380	25	18.0	25	15.9	1281
		1550	25	18.2	40	13.0	805
W 99.7 % – C_{60} 0.3 %	5.3	1220	37	17.1	–	7.3	348
		1380	37	17.1	–	5.1	339
		1550	37	17.0	–	3.2	261

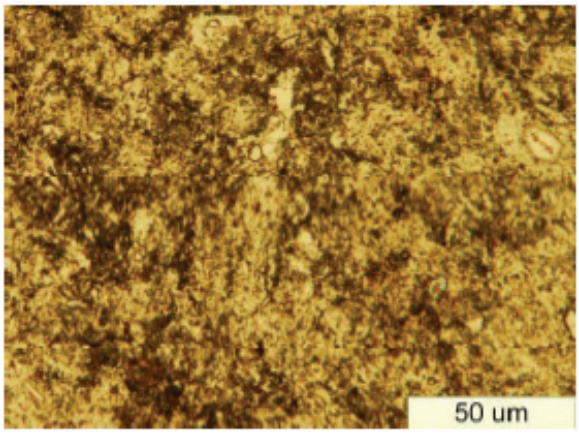

Fig. 3. Sintered W powder (polished section), light areas indicate reduced density of the compact [25]

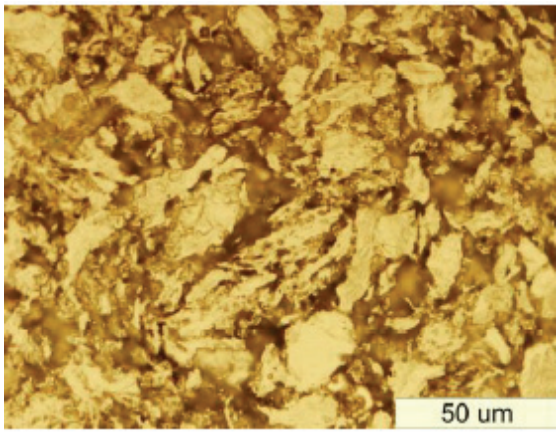

Fig. 4. Sintered tungsten powder with DND addition (0.3 wt. %), temperature 1200 °C; light areas correspond to W–DND conglomerates [25]

2) forming the specimen of the future compact from the milled powder;

3) sintering of the formed sample;

4) polishing and grinding of the obtained compact for surface characterization.

The initial powders were ground in a planetary mill. The formed samples were sintered at various temperatures under a pressure of 5.3 GPa. The resulting compacts were cylindrical, with a diameter of 4.5 mm and a height of up to 4.6 mm.

For the obtained samples (before and after sintering), the crystallite size, density, microhardness, and elastic modulus were determined (Table 2) [25].

Table 2 demonstrates a decrease in the hardness of sintered tungsten (W) with increasing sintering temperature.

Figure 3 shows a sample of pure tungsten (sintering temperature T_{sint} = 1200 °C); the light spots correspond to regions of reduced density.

With the addition of 0.3 wt. % DND, sintering had virtually no effect on grain size, and the density of the material also remained nearly unchanged. However, the microhardness of the compact increased significantly–by a factor of 1.7–2.2 (Fig. 4). At the same time, the stiffness (rigidity) of the compact increased by a factor of 2.8–4.5.

Since the size of nanodiamonds is smaller than the size of dislocations, they hinder crack propagation in the compact and reduce recrystallization of tungsten. The introduction of fullerenes (0.3 wt. %) into the composition of sintered tungsten powder leads to a reduction in tungsten grain size; however, at the same time the main properties of the compact deteriorate, namely hardness, strength, and density.

Thus, the authors of [25] showed that sintering tungsten with a small amount of nanodiamonds allowed an increase in the microhardness of the compacts by 1.5–2.0 times, while the Young's modulus increased by almost 4 times.

In [21], tungsten powder grade PVV (TU 48-19-72-92) with a particle size of 0.8–1.7 μm was used to obtain samples. DND produced by the FSUE "SKTB "Technolog", (St. Petersburg, Russia), obtained from tetryl in accordance with TU 3974-456-05121441-2008, were used as an additive. The DND had an average particle size of 3.5–6.5 nm and a specific surface area of (310 ± 10) $m^2 \cdot g^{-1}$. Highly purified DND with a non-combustible residue content of 0.6 wt. % was used, as well as DND doped during synthesis with amorphous boron in an amount of 2 wt. %.

The powder mixture consisting of tungsten powder and 0.3 wt. % DND additive (5 at. %) was activated with a power density of 3 $W \cdot g^{-1}$ in a planetary ball mill using steel balls 5 mm in diameter in a hardened steel drum. Based on the activated mixture, cylindrical compacts with a diameter of 4.5 mm and a height of 5–6 mm were produced by pressing. These were then sintered in a high-pressure apparatus at 4.5 GPa in the temperature range of 1200–1500 °C with a holding time of 10 s. For comparison, compacts from pure tungsten powder without DND addition were produced under the same sintering conditions.

The microhardness (H_μ) of the sintered compacts was measured using a PMT-3 microhardness tester by the Vickers method under a load of 200 g. The fracture toughness (K_{1c}) of the compacts was also evaluated using the indentation method.

It was found that the shrinkage of compacts sintered without DND additives is 5–10% higher compared to samples obtained from powder mixtures containing DND.

As a result of thermobaric sintering in the temperature range of 1300–1400°C, compacts based on "pure" tungsten were obtained with a microhardness H_μ in the range of 3.3–3.8 GPa. An increase in sintering temperature to 1500 °C contributed to a decrease in material porosity and an increase in microhardness up to 5.5–5.7 GPa, with fracture toughness at the level of 5.5–6.5 $MPa \cdot m^{1/2}$.

At the same time, the introduction of a 0.3 wt. % DND additive led to an increase in H_μ to 8–11 GPa, which is 2.5–3 times higher than the microhardness of compacts without DND addition (Table 3).

During indentation of compacts with DND additives, no cracks were observed on the polished surfaces, which may indicate relatively high fracture toughness of the sintered material.

X-ray diffraction studies confirmed the presence of tungsten and "traces" of DND in the sintered compacts, with no graphite phase detected (Fig. 5). Comparative studies of the fine structure of the compacts showed a reduction in tungsten crystallite size (L) in samples with DND compared to compacts of "pure" tungsten (57 nm and 103 nm, respectively). A decrease in the tungsten lattice parameter was also observed (a = 3.1648 Å for pure tungsten samples and a = 3.1635 Å for samples with DND), indicating the formation of a carbon solid solution in tungsten.

Analysis of the X-ray diffraction patterns showed that the sintered samples predominantly developed crystallographic planes in the {211} direction, which is consistent with atomic force microscopy data and indicates plastic deformation of tungsten grains (Fig. 6).

Table 3. Results of microhardness studies of compacts [21]

Composition of the composite, wt. %	Sintering pressure P, GPa	Cell temperature T, °C	Sintering time t, s	Microhardness H_μ, GPa
100 % W	4.5	1300	10	3.3
		1400		3.8
		1500		5.5–5.7
99.7 % W +0.3 % DND	4.5	1200	10	6–7
		1300		9–11
		1400		8–9.7
		1500		6.5–7.5
99.7 %W +0.3 % DND (boron)	4.5	1200	10	7–8
		1300		11.5–15.5
		1400		11.5–12.7
		1500		8.5–10

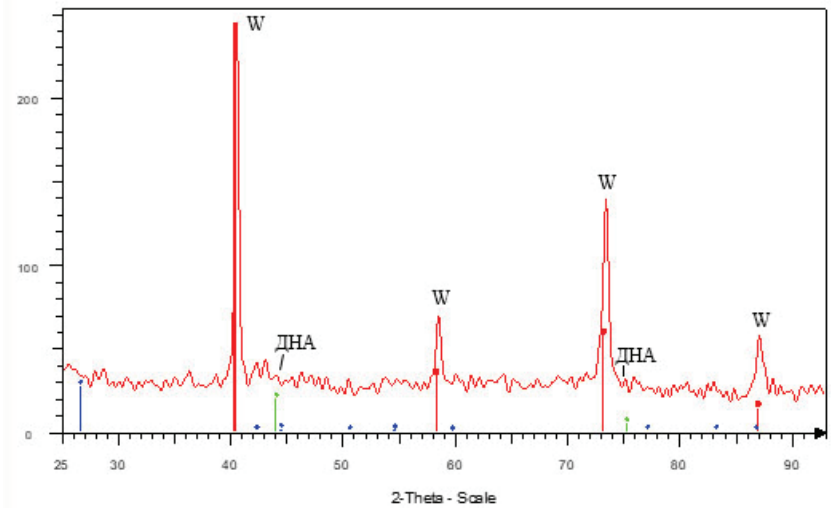

Fig. 5. Fragment of the diffraction pattern of a tungsten-based compact with 0.3 wt. % DND addition, obtained at a pressure of 4.5 GPa, temperature of 1300 °C, and holding time of 10 s

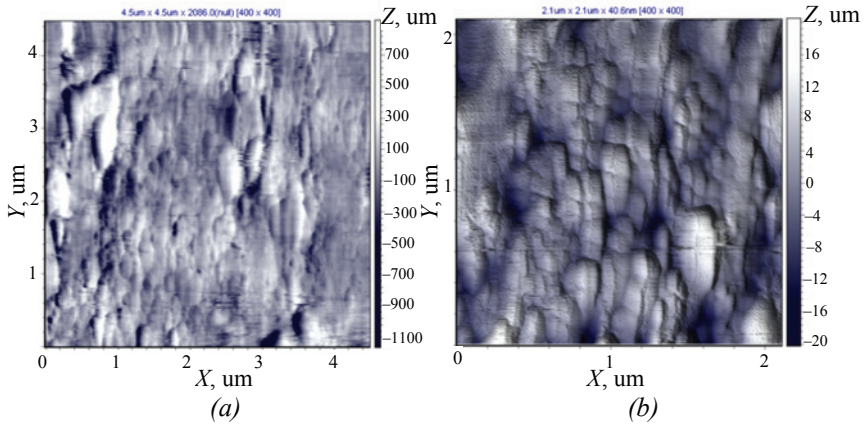

(a) *(b)*

Fig. 6. Microstructure of a tungsten-based compact with 0.3 wt. % DND addition, obtained at a pressure of 4.5 GPa, temperature of 1300 °C, and holding time of 10 s:
a – lateral contrast image; *b* – topography of the submicrocrystalline structure [21]

After deformation, tungsten grains predominantly acquire an elongated shape, with a size ranging from 100 to 500 nm (Fig. 6*a*, *b*). At the grain boundaries, inclusions are observed (presumably aggregates of DND particles) with a size of up to 30 nm (Fig. 6*a*).

Under isothermal holding of 10 s, an increase in sintering temperature leads to a decrease in the microhardness of the compacts (Table 3), which is attributed to grain growth of tungsten [25]. Further increase of isothermal holding time beyond 15 s in the temperature range of 1300–1400 °C also contributes to a reduction in microhardness to 5.8–6.5 GPa.

At 1300°C, increasing the isothermal holding time to 45–135 s, on the contrary, leads to an increase in H_μ to 8–10 GPa. As noted in [26–28], the increase in microhardness in this case occurs due to the formation of tungsten carbides. The tungsten lattice parameter decreases to 3.1625 Å, while tungsten crystallites grow to a size of 138 nm.

Higher H_μ values are exhibited by samples obtained with boron-doped DND additions (Table 3). In this case, the resulting material is characterized by pronounced structural heterogeneity, which manifests itself in a wider range of measured H_μ values (Fig. 7*c*).

An increase in the sintering temperature of compacts with boron-doped DND above 1400°C leads to their embrittlement, as evidenced by the appearance of cracks during sample indentation. Structural studies of the compacts revealed the presence on the polished surfaces of plate-like particles with a hexagonal shape (Fig. 7*c*), indicating the formation of refractory compounds based on the W–C–B system at these temperatures [29].

Thus, the use of high-pressure techniques in combination with DND enabled the production of tungsten-based compacts with a submicrocrystalline structure and microhardness levels of 10–11 GPa and

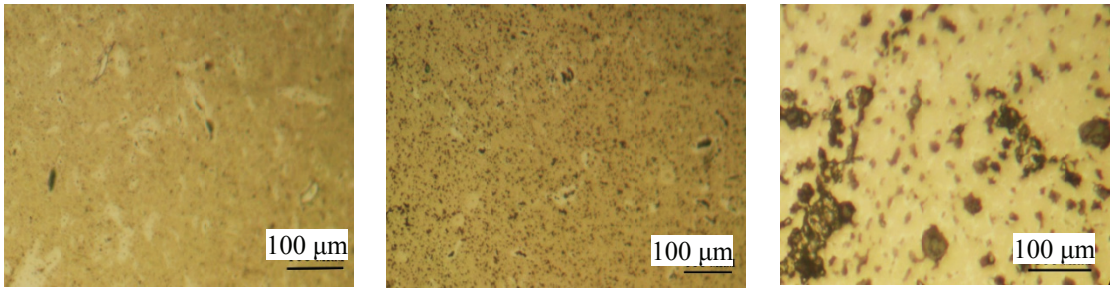

(a) *(b)* *(c)*

Fig. 7. Structure of compacts after sintering for 10 s:
a – addition of deeply purified DND, sintering temperature 1300 °C; *b* – boron-doped DND addition, sintering temperature 1300 °C; *c* – boron-doped DND addition, sintering temperature 1400 °C [21]

11.5–15.5 GPa for samples containing 0.3 wt. % deeply purified DND and samples containing 0.3 wt. % boron-doped DND, respectively. At the same time, deeply purified DND improves the ductility of the resulting material, whereas boron-doped DND increases its brittleness due to possible boride formation.

In [30], the possibility of producing lightweight pseudo-alloys based on tungsten was investigated. Tungsten pseudo-alloys with lighter metals such as Cu, Fe, and Ni are well known [31].

The resistance of tungsten pseudo-alloys to high-temperature creep and heat resistance is ensured by the fact that nanoparticles hinder dislocation motion and stabilize the sintered structure.

In [30], strengthening of pseudo-alloys was achieved by introducing powders of DND, ASh (produced by FSUE "SCTB "Tekhnolog"), and multi-walled carbon nanotubes (MWCNTs) (produced by JSC "ZAVKOM", Tambov) into mixtures of tungsten powder with copper and/or aluminum.

Analysis of the data in Table 4 shows that DND treated at 650°C in the absence of air partially de-agglomerates, and its introduction into aluminum powder at a level of 10 wt. % (experiment 1, Table 4) results in a non-pressable mixture (2000 atm); the sample disintegrates after removal of the pressing load. Thus, fully molten aluminum cannot wet the entire surface of the DND.

Table 4. Characteristics of tungsten/aluminum (DND) compacts, ∅ 25 mm [30]

Experiment No.	Pressed composition (ratio), wt. %, process conditions	Actual density, g·cm^{-3}	Porosity, vol. %	Hardness HB (pressed at room conditions)	Tablet annealing at 700 °C after pressing	Notes
1	Al + 10 % DND standard powder (650 °C), t = 750 °C					The sample disintegrated after pressing
2	W/Al (70/30), t = 750 °C + + 0.3 wt. % DC	5.11	24.7	21.5	Partially disintegrated after annealing	
3	Al/W (33/67), t = 750 °C + + 0.3 wt. % DND (Ioffe Institute)	3.29	51.5	27.9	Withstood annealing, HB = 27.1	Sent for annealing at 1220 °C
4	Al/W (90/10) +0.58 wt. % DND (Ioffe Institute), t = 630 °C	2.32	21.5	20.0	Did not settle, h = 20 mm, d_{av} = 25 mm	The powder composition breaks down after heating.
5	Al/W (90/10), +0.58 wt. % DND (Ioffe Institute) + + MWCNTs (0,6 wt. %), t = 630 °C	2.13	27.9		Cracked after holding at 700 °C	

The introduction into a tungsten–aluminum mixture (70/30, respectively) of another allotropic form of carbon–detonation diamond-containing charge (ASh) (experiment 2, Table 4) –at a low concentration of 0.3 wt. % (with ~70 % DND content in ASh) made it possible to obtain a sufficiently strong compact with a Brinell microhardness HB of 21.5, but with high porosity of 24.7 %. However, after annealing at 750 °C, the compact partially disintegrated.

In experiment 3 (Table 4), a sample consisting of a mixture of aluminum (33 wt. %), tungsten (67 wt. %), and 0.3 wt. % DND (above 100 %), modified using the Ioffe Institute technology (DND particle size ~4 nm in a 0.5 wt. % aqueous suspension), was pressed at 3000 atm. The resulting compact before annealing had a relatively high microhardness of 27.9 HB (and very high porosity of 51.5 %), and after annealing at 700 °C, the sample showed no visible changes and the microhardness remained almost unchanged at 27.1 HB.

In experiments 4 and 5 (Table 4), compositions with a significant predominance of Al over W (with only ~10 wt. % W) were studied under 2000 atm pressing. In experiment 4, the compact had a microhardness of 20 HB with relatively high porosity of 21.5 vol. %, using an addition of ~0.6 wt. % DND modified at the Ioffe Institute. However, after heating at 630 °C, the compact disintegrated. In experiment 5, multi-walled carbon nanotubes (MWCNTs) were additionally introduced in an amount of 0.6 wt. % into the composition of experiment 4, which further deteriorated the compact; after annealing, the sample cracked.

Table 5 presents the properties of three-component systems based on copper, tungsten, and aluminum with DND additions ranging from 0.3 to ~0.6 wt. %. For some samples, no pre-pressing thermal treatment of the powder mixture was used (experiments 1–3), while for others, thermal treatment at 630 °C in an argon atmosphere was applied. Considering the large difference in densities of the metals used (Al:Cu:W), where Al is 7.1 times and Cu is 2.1 times lighter than W, it is difficult to expect the formation of a sufficiently homogeneous pseudo-alloy with high intermetallic adhesion, although such a material would have broad application potential.

Table 5. Characteristics of compacts tungsten/copper/aluminum/nanodiamond, ∅ 25 mm, 2000 atm, aqueous DND suspension [30]

Experiment No.	Pressed composition (ratio), wt. %, process conditions	Theoretical density (non-porous), g·cm^{-3}	Actual density, g·cm^{-3}	Porosity, vol. %	Hardness HB, without heating after pressing	Annealing at 700 °C, after pressing
	Without heat treatment of the initial powder mixture					
1	W/Cu/Al = 75/5/20 + DND (Ioffe Institute); (0.58 %)	8.44	6.10	27.7	22.5 HB	After annealing, a small amount of golden-silver powder is present on the surface
2	W/Cu/Al=20/55/25 + DND (Ioffe Institute); (0.58 %)	6.08	5.62	7.6	24.0 HB	After 700 °C (argon, 1 h) the compact cracked
3	W/Cu/Al = 50/25/25 + DND (Ioffe Institute); (0.58 %)	6.83	5.14	24.7		After 700 °C (argon, 1 h) the compact partially disintegrated
	Heat treatment of the initial powder mixture (630 °C, argon, 1 h)					
4	W/Cu/Al = 35/50/15 + DND (Ioffe Institute); (0.58 %)	7.71	6.03	21.8		Sintered; did not fall apart, but the appearance is non-uniform subjected to annealing at 1220 °C
5	W/Cu/Al=35/50/15 + + Standard aqueous DNA suspension, (0.3 %)	7.71	5.89	23.6		Monolithic sintered body subsequent annealing (Table 6)

Experiment 1 (Table 5) showed relatively high microhardness of 22.5 HB and medium porosity of 27.7 vol. %. However, due to ambiguous results after annealing at 700 °C, the composition was not further used.

A reduction in tungsten content (almost fourfold) compared to experiment 1 (from 75 to 20 wt. %) in experiment 2 (Table 5) resulted in very low porosity of 7.6 vol. % and relatively high microhardness of 24.0 HB. However, after thermal treatment at 700°C in argon, the sample failed and cracked.

Experiment 3 (Table 5) also did not yield a strong compact; after thermal treatment at 700 °C, the compact partially cracked.

In experiments 4 and 5, aqueous DND suspensions were used to treat the metal powders separately rather than jointly, as in previous cases. After water removal, the powders were mixed. The porosity of the resulting compacts remained relatively high (22–24 vol. %), but after sintering at 700 °C, no disintegration or damage of the compacts was observed, and they were subsequently subjected to vacuum sintering at 1220 °C.

Next, the authors, having observed the low wettability of metal powders with aqueous DND suspensions, replaced water with isopropyl alcohol (IPA) and found high wettability for W, Cu, and Al. IPA containing DND readily penetrates into the pores of metal powders, delivering nanodiamonds into them, and is easily removed afterward. This makes it possible to ensure uniform distribution of nanodiamonds throughout all pores of the powders, which is important for subsequent pressing and thermal treatment at 1220 °C.

Before pressing, each metal was impregnated separately; after removal of IPA, each metal was thoroughly ground by mechanical rubbing. After mixing the metals with DND, the mixture was again carefully homogenized. Pressing was then carried out at 3000 atm.

From the data in Table 6 it can be seen that thermal treatment at 1220 °C in a vacuum furnace of binary and ternary systems (based on W, Al, and Cu) with DND additions preserved the integrity of the compacts and increased their microhardness by 2–3 times compared to previous experiments (Tables 4 and 5). However, the high porosity of the sample in experiment 4 (Table 6) led to embrittlement and failure of the specimen during microhardness testing.

Experiments showed that among the studied forms of carbon nanomaterial allotropy (DND, graphene, and nanotubes), the most effective additive was DND pre-treated at 650 °C. The stability of the samples (Table 6) to heat treatment at 1220 °C was not affected by their high porosity.

As a result, the authors of [30] obtained two new types of lightweight pseudo-alloys – binary and ternary systems containing tungsten. One of them contains 10 wt. % W, 90 wt. % Al, and 0.3 wt. % nanodiamond (above 100 %), and has a microhardness of 60.2 kg·mm^{-2}.

Table 6. Main parameters of W/Cu/Al/DND press-sintered compacts, ∅ 20 mm, annealing temperature 1220 °C [30]

Experiment No.	Pressed composition (ratio), wt. %, process conditions	Mass (table), g Diameter, mm	Theoretical density (non-porous), g·cm^{-3}	Actual density, g·cm^{-3}	Porosity, vol. %	Notes, HB
1	W/Al = 10/90, DND (650 °C), suspensions in IPA, ∑ DND 0.3 wt. %.	19.75 ∅25.06	2.95	2.55	13.6	∅25, *h* = 17 mm, the sample was preserved; HB 60.2
2	W/Cu/Al = 35/50/15, ∑ 1.2 % DND (650 °C) in IPA	20.10 ∅20.2	7.71	4.94	35.9	After annealing at 1220 °C, the sample was preserved; HB 94.1
3	W/Al = 10/90 DND (Ioffe Institute) 0.45 %	22.30 ∅20.10	2.95	2.28	22.7	The sample was preserved; HB 40.2
4	W/Cu = 65/35, DND (Ioffe Institute) 0.45 %	19.45 ∅20.20	13.73	7.78	43.3	The sample was preserved, but cracked during microhardness testing

The other contains 35 wt. % W, 50 wt. % Cu, 15 wt. % Al, and 1.2 wt. % DND, and has a microhardness of 94.1 $kg \cdot mm^{-2}$. These compositions are easily machinable and have smooth, glossy surfaces.

9. Possibility of using nanodiamonds in photonics

The authors of [32] aimed to test the possibility of using such a complex but promising product as DND crystallites as a nonlinear light scatterer in hydrosols. It was shown that the decrease in transmittance of nanodiamond hydrosols under optical limiting (OL) of pulsed laser radiation is caused by an increase in nonlinear scattering. At the same time, nanodiamond hydrosols exhibit high stability under high-power laser exposure. In addition, under prolonged and intense laser irradiation (~1 $GW \cdot cm^{-2}$), nanodiamond hydrosols demonstrate high optical stability – no aggregation of crystallites was observed.

In [33], it was found that the nonlinear transmittance coefficient of DND hydrosols is independent of polarization. The results of [32, 33] show that nanodiamond hydrosols are suitable for use as optical limiters of laser radiation.

In [34, 35], the authors demonstrated the possibility of producing films from nanodiamond hydrosols on glass substrates and laser recording of images on them. Under laser irradiation, the semi-transparent films darken, accompanied by a decrease in background luminescence.

In [36], nanodiamond hydrosols with aggregate sizes of 50, 110, and 320 nm were investigated. It was shown that the size of DND aggregates influences both the optical limiting (OL) characteristics and the stability of the hydrosol under laser irradiation. Nanodiamond aggregates in hydrosols with a size of 320 nm exhibit significantly better OL performance than DND aggregates with a size of 50 nm. In addition, such hydrosols can be used for smooth control of laser pulse duration.

In [37], nanodiamonds were introduced into heavy water (D_2O), and a nanodiamond colloidal sol was proposed as a nonlinear optical filter for the telecommunication range. The resulting nanodiamond sol in heavy water exhibits high beam and colloidal stability.

In [38], the authors studied the optical limiting behavior of nanodiamonds with surface-grafted amino and hydrogen functional groups under exposure to nanosecond Nd:YAG laser pulses. It was shown that nonlinear attenuation in DND-H is significantly greater than attenuation in DND-NH_2.

The authors of [32–38] demonstrated the strong potential of nanodiamonds for generating nonlinear optical effects.

10. Possible use of nanodiamonds in crop production

The problem of increasing crop yield and disease resistance in plant cultivation has always been and will remain a key issue in agriculture across all countries. In [39], in order to protect plant seeds from diseases and preserve nutrients, the authors developed a technology for applying a protective porous film (a silica shell) using aqueous sols based on tetraethoxysilane $Si(OEt)_4$. Based on tetraethoxysilane (TEOS), later in [40] the compositions were significantly expanded, and sol-gel systems were developed containing solutions of micro- and macroelements, as well as DND or ASh, where the latter was doped with amorphous boron during detonation synthesis (produced by FSUE "SCTB "Tekhnolog" St. Petersburg, Russia) [41].

Figure 8 shows SEM-images of barley seed surfaces (*a* – untreated, *b* and *c* – treated with silica using different TEOS concentrations), and Fig. 9 shows SEM-images of Chinese cabbage seeds treated with TEOS in the same proportions as in Fig. 8.

The most significant result was the use of boron-doped ASh for modifying silica sols, which led to the formation of plants with high biomass.

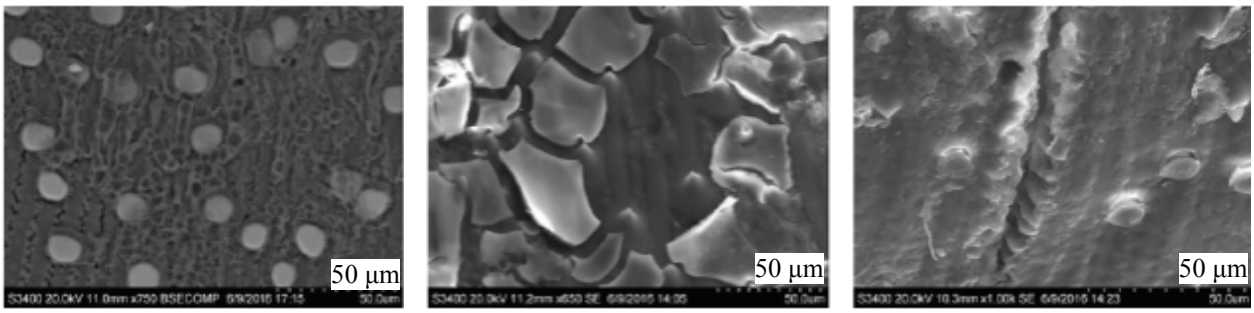

(a) *(b)* *(c)*

Fig. 8. SEM-images of spring barley seeds:
a – untreated; *b* and *c* – treated with silica sols containing 1 wt. % and 20 wt. % TEOS, respectively [40]

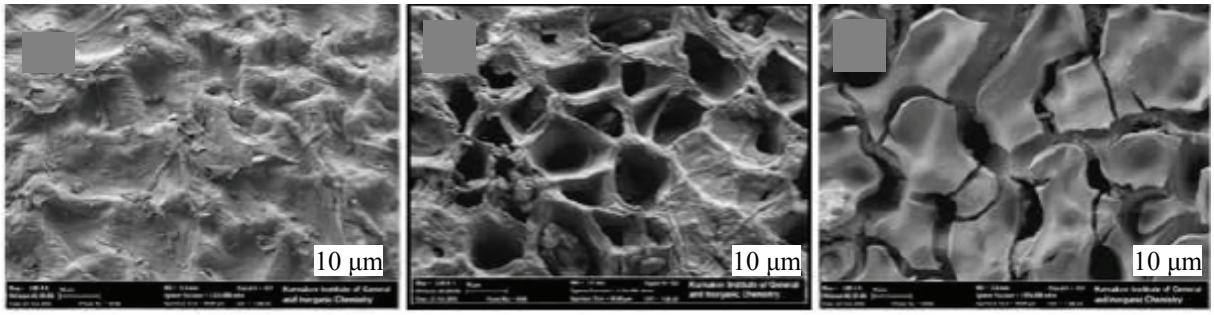

(a) *(b)* *(c)*

Fig. 9. SEM-images of Beijing cabbage seeds:
a – untreated; *b* and *c* – treated with silica sols containing 1 wt. % and 20 wt. % TEOS, respectively [40]

Thus, ASh (boron) was tested as a biologically active additive (0.05–0.1 wt. %) for pre-sowing treatment of Chinese cabbage seeds (variety Daqingkou, China, k – 56). As a result, a statistically significant positive effect of the aqueous suspension of ASh (boron) (0.05–0.1 wt. %) was observed on the following seedling characteristics (compared to the control): seed germination energy and germination rate of Chinese cabbage increased by approximately 50–70 % [42].

A significant positive effect of ASh (boron) on the morphological characteristics of Chinese cabbage plants at early growth stages was also observed when using ASh-boron for pre-sowing seed treatment in combination with silica (increase in shoot length by ~20 % and root length by ~50 % compared to the control), as well as an increase in plant biomass by ~100 % (20 days after planting treated seeds).

11. Oils and lubricants. Space lubricants with DND

Components and mechanisms of spacecraft operate under extreme space conditions, including high vacuum, radiation, and low and high temperatures [43, 44]. Space lubricants (SL) for friction units are formulated from thickened synthetic oils with various functional additives. However, under the influence of penetrating radiation and elevated temperatures (up to ~150 °C), undesirable chemical reactions may occur on tribological contact surfaces, including thermal degradation of the lubricant.

The introduction of ASh into SL (0.2–5.0 wt. %) according to [45] helps to suppress such destructive processes. Table 7 presents the studied lubricant compositions, while Table 8 shows the results of key

Table 7. Composition of main lubricant components [45]

Name	Content in composition, wt. %				
	1	2	3	4	5
Diamond-graphite nanopowder (NP)	0.20	0.75	1.50	3.00	5.00
Diamond NP	0.05	0.188	0.375	0.75	1.25
Graphite NP	0.15	0.562	1.125	2.25	3.75
Tin sulfate SnO_4	1.00	5.0	10.0	15.0	17.0
Soap-based plastic lubricant	98.80	94.25	88.50	82.00	78.0

Table 8. Main characteristics of tested lubricants on the SMT-1 friction testing machine [45]

Composition of lubricants	Maximum specific load, MPa	Friction coefficient	Wear rate, $10 \cdot 10^{-6}$ kg·m^{-3}
1	26.3	0.062	59.4
3	3.3	0.050	30.2
5	21.4	0.063	57.5
Lubricant VNIINP-232 Russian Standart 14068-79	23.5	0.059	66.0

performance characteristics of the proposed lubricants. It was shown that the coefficient of friction decreases by 12–15 %, and wear of mating steel components is reduced by a factor of 2.

DND nanoparticles remove micro-asperities from steel contact surfaces, increasing the real contact area. At the same time, nanodiamond crystallites also penetrate microcracks on the surfaces of contacting parts, strengthening them. The non-diamond graphite-like carbon also contributes to reducing friction by filling the oil film.

12. Application of nanodiamonds for improving internal combustion engine lifetime

Improving the service life of machines and mechanisms strongly depends on enhancing the quality of lubricants and oils, including the introduction of various additives into them [46, 47]. To eliminate metallic contact between mating components and to form a reliable boundary lubrication layer, additives of ultrafine solid particles are often used in oils and greases, providing high anti-friction and anti-wear properties to the lubricating composition [48]. At the recommended minimum concentrations of such additives (0.01–0.5 wt. %), the physico-chemical properties of lubricants and oils remain practically unchanged, and the operating temperature range of such lubricants is wide. These additives exhibit a pronounced positive effect both on the contact surfaces and on the characteristics of the boundary and lubricating layers [49]. The use of ultradisperse additives makes it possible to eliminate oil-soluble additives.

Layered fillers have often been used, such as molybdenum disulfide, graphite, soot, and sometimes metal powders and their compounds; however, the particle size of these additives is relatively large (1–20 μm) [50]. In this context, the use of DND with individual crystallite sizes of 4–8 nm is a logical development. DND are characterized by low chemical reactivity, a high specific surface area (300–400 m²/g), and an almost spherical shape [46]. In addition, due to their high surface energy, DND exhibit a strong structuring effect in lubricating compositions. They significantly enhance the physico-mechanical properties of lubricant films.

The running-in process of mating surfaces under the influence of diamond-containing oil additives is completed when the contact area reaches a hydrodynamic lubrication regime. In this case, closed liquid-crystalline structures are formed, which contribute to an increase in the load-bearing capacity of the contact.

In plastic lubricants, nanodiamonds, due to their strong structuring ability, form a load-bearing framework structure.

13. Fuel. Influence of detonation nanodiamonds on the combustion process of model composite solid rocket propellants

In [51], the authors evaluated the combustion of various fuel compositions containing nanodiamonds. A total of 14 formulations were prepared, and the laws of burning rates were determined; five of the compositions are presented in Table 9.

Among 14 formulations, different forms of carbon nanomaterial allotropy were tested, including: standard DND powder (DND-STP); DND-STP treated at various temperatures without air access (450, 650, 900 °C); nanocrystalline DND (4 nm) produced by the Ioffe Institute method; charcoal; graphite nanopowder; oxidized few-layer graphene; and ground adamantane powder.

It was found that DND increases the burning rate of the fuel compositions, with the highest increase of 23 % achieved when modified nanodiamond is introduced. At the same time, the combustion temperature decreases by approximately 200 °C, which has a positive effect on engine lifetime. It is assumed that DND particles do not fully oxidize to carbon dioxide during combustion, but are instead partially converted only to low-molecular-weight CO.

The introduction of DND into the fuel promotes the formation of a fractal carbon system, with a carbon framework emerging at the combustion surface, thereby providing high thermal conductivity of the composition.

14. Conclusion

It was shown that oriented sintering of DND (~5 nm) makes it possible to obtain monocrystallites of significant size (~80 μm). New, safer contrast agents based on DND grafted with gadolinium and manganese for MRI were developed. The effectiveness of DND as a material for diffuse reflection of very cold neutrons was demonstrated. The results of creating europium luminescent centers in CVD diamond films using DND precursors with europium deposited on their surface were described.

It was established that DND nanoparticles in liquid media form branched fractal structures with a dimensionality of d_m = 1.7–2.2 (in water and oils). A universal powder additive based on DND for electroplating processes was developed, providing coating quality significantly superior to previously achieved results.

Table 9. Investigated compositions of fuel formulations [51]

Composition number	Composition, %		Dependence $U(p)$, mm·s^{-1}	U_{40}, mm·s^{-1}	U_{100}, mm·s^{-1}	U_{150}, mm·s^{-1}
1	Binder Oxidizer Plasticizer	28 70 2	$615p^{0.315}$	19.7	26.2	29.8
2	Binder Oxidizer Modified DND Plasticizer	26 70 2 2	$2.585p^{0.549}$	19.6	32.4	40.5
3	Binder Oxidizer DND (650 °C)	28 70 2	$2.676p^{0.529}$	18.9	30.6	37.8
4	Binder Oxidizer DND (4 nm)	28 70 2	$3.031p^{0.508}$	19.8	31.4	38.5
5	Binder Oxidizer DND (900 °C)	28 70 2	$2.844p^{0.505}$	18.4	29.1	35.6

U – Burning rate of fuel compositions at different pressures in the combustion chamber.

Based on tungsten powder and DND, new high-quality sintered compacts were developed, and the use of DND in lightweight tungsten-based pseudo-alloys made it possible to obtain new high-quality lightweight tungsten–aluminum and tungsten-copper-aluminum alloys.

The nonlinear optical properties of nanodiamonds in aqueous suspension were demonstrated, enabling their use as optical power limiters. The application of an aqueous suspension of boron-doped diamond-containing charge for pre-sowing treatment of Chinese cabbage resulted in an approximately 100 % increase in plant biomass.

The effectiveness of diamond-containing charge as an additive in plastic space lubricants was demonstrated, reducing wear of mating parts by a factor of 2, and by a factor of 2.2 for ground transport components. DND additives in model paste-like fuels increase the combustion rate by 23 %, while the temperature of combustion products decreases by approximately 200 °C.

15. Funding

The present study did not receive any external funding.

Финансирование

Настоящее исследование не получило внешнего финансирования.

16. Conflict of interests

The authors declare no conflict of interest.

Конфликт интересов

Авторы заявляют об отсутствии конфликта интересов.

References

1. Volkov KV, Danilenko VV, Elin VI. Synthesis of diamond from the carbon in the detonation products of explosives. *Combustion, Explosion and Shock Waves*. 1990;26(3):366-368. DOI:10.1007/BF00751383

2. Danilenko VV. *Explosion: physics, engineering, technology*. Moscow: Energoatomizdat; 2010. 784 p. (In Russ.)

3. Dolmatov VYu. *Detonation nanodiamonds. Preparation, properties, application*. Saint Petersburg: Professional; 2011. 536 p. (In Russ.)

4. Titov VM, Anisichkin VF, Mal'kov IYu. Synthesis of ultradispersed diamond in detonation waves. *Combustion, Explosion and Shock Waves*. 1989;25(3):372-379. DOI:10.1007/BF00788819

5. Ershov AP, Satonkina NP, Dibirov OA, Tsykin SV, et al. A study of the interaction between the components of heterogeneous explosives by the electrical-conductivity method. *Combustion, Explosion and Shock Waves*. 2000;36(5):639-649. DOI:10.1007/BF02699528

6. Yur'ev GS, Dolmatov VYu. X-ray diffraction analysis of detonation nanodiamonds. *Journal of Superhard Materials*. 2010;32(5):311-328. DOI:10.3103/S1063457610050035

7. Kidalov SV, Shahov FM, Shvidchenko AV, Smirnov AN, et al. Growth of diamond microcrystals by the mechanism of oriented attachment at high pressure and temperature. *Pis'ma v zhurnal tehnicheskoj fiziki = Technical Physics Letters*. 2017;43(1):21-29. DOI:10.21883/PJTF.2017.01.44085.16417 (In Russ.)

8. Barnard AS. Self-assembly in nanodiamond agglutinates. *Journal of Materials Chemistry*. 2008;18(34):4038-4041. DOI:10.1039/b809188a

9. Kidalov SV. *Phase transitions graphite-diamond in carbon nanostructures at high pressures and temperatures*. Available from: https://www.ioffe.ru/serve/theses/avtoref/Thes_0578.pdf [Accessed 15 January 2026] (In Russ.)

10. Panich AM, Salti M, Goren SD, Yudina EB, et al. Gd(III)-grafted detonation nanodiamonds for MRI contrast enhancement. *The Journal of Physical Chemistry C*. 2019;123(4):2627-2631. DOI:10.1021/acs.jpcc.8b11655

11. Panich AM, Shames AI, Aleksenskii AE, Yudina EB, et al. Manganese-grafted detonation nanodiamond, a novel potential MRI contrast agent. *Diamond and Related Materials*. 2021;119:108590. DOI:10.1016/j.diamond.2021.108590

12. Panich AM, Aleksenskii AE, Yudina EB, Vul' AYa. Spatially resolved spin–lattice relaxation times and line widths in manganese-grafted detonation nanodiamonds. *The Journal of Physical Chemistry C*. 2022;126(3):1489-1495. DOI:10.1021/acs.jpcc.1c09026

13. Aleksenskii A, Bleuel M, Bosak A, Chumakova A, et al. Effect of particle sizes on the efficiency of fluorinated nanodiamond neutron reflectors. *Nanomaterials*. 2021;11(11):3067. DOI:10.3390/nano11113067

14. Aleksenskii A, Bleuel M, Bosak A, Chumakova A, et al. Clustering of diamond nanoparticles, fluorination and efficiency of slow neutron reflectors. *Nanomaterials.* 2021;11(8):1945. DOI:10.3390/nano11081945

15. Yudina EB, Aleksenskii AE, Bogdanov SA, Bukalov SS, et al. CVD nanocrystalline diamond film doped with Eu. *Materials*. 2022;15(16):5788. DOI:10.3390/ma15165788

16. Kuznetsov NM, Belousov SI, Kamyshinsky RA, Vasiliev AL, et al. Detonation nanodiamonds dispersed in polydimethylsiloxane as a novel electrorheological fluid: Effect of nanodiamonds surface. *Carbon*. 2021;174:138-147. DOI:10.1016/j.carbon.2020.12.014

17. Dolmatov VY. Detonation-synthesis nanodiamonds: synthesis, structure, properties and applications. *Russian Chemical Reviews*. 2007;76(4):339-360. DOI:10.1070/RC2007v076n04ABEH003643

18. Dolmatov VYu, Rudenko DV, Burkat GK, Aleksandrova AS, et al. A study of the process of gold plating from citrate and phosphate electrolytes in the presence of modified detonation nanodiamonds. *Journal of Superhard Materials*. 2019;41(3):169-177. DOI:10.3103/S1063457619030043

19. Dolmatov VYu. Bogdanov SP, Marchukov VA, Vehanen A, et al. A powder composition containing detonation nanodiamonds (DNDs) is an effective additive to the electrolyte of wear–resistant chrome plating. *XXXIV Symposium "Modern Chemical Physics". Collection of reports. September 16-25.* Tuapse; *2022*, p. 191-192. (In Russ.)

20. Myllymäki V, Vehanen A, Dolmatov VYu, Burkat GK, et al. Electrochemical anode oxidation of aluminum in the presence of detonation diamond-containing carbon. *Book of abstracts of 4th International scientific-practical conference "Graphene and related structures: synthesis, production, and application". October 6-8.* Tambov; *2021*, p. 95-97. (In Russ.)

21. Senyut' VT, Kovaleva SA, Dolmatov VYu, Vityaz' PA, Grigor'ev IE. Investigation of the effect of nanodiamond additives on the structure and microhardness of a sintered tungsten-based composite. *New materials and technologies: powder metallurgy, composite materials, protective coatings, welding: materials of the 16th International Scientific and Technical Conference (Minsk, May 22-24, 2024), National Academy of Sciences of Belarus.* Minsk: Belarusskaya Nauka; 2024. p. 291-293. (In Russ.)

22. Rieth M, Boutard JL, Dudarev SL, Ahlgren T, et al. Review on the EFDA programme on tungsten materials technology and science. *Journal of Nuclear Materials*. 2011;417(1-3):463-467. DOI:10.1016/j.jnucmat.2011.01.075

23. Levin ZS, Hartwig KT. Strong ductile bulk tungsten. *Materials Science and Engineering: A*. 2017;707:602-611. DOI:10.1016/j.msea.2017.09.100

24. Dine S, Bernard E, Herlin N, Grisolia C, et al. SHS synthesis, SPS densification and mechanical properties of nanometric tungsten. *Metals*. 2021;11(2):252. DOI:10.3390/met11020252

25. Zharchenkova MI, Perfilov SA, Lomakin RL. Investigation of the physico-mechanical properties of nanostructured tungsten modified with carbon nanoclusters. *ChemChemTech.* 2014;57(5):74-76. (In Russ.)

26. Chernozatonskii LA, Sorokin PB, Kuzubov AA, Sorokin BP, et al. Influence of size effect on the electronic and elastic properties of diamond films with nanometer thickness. *The Journal of Physical Chemistry C*. 2011;115(1):132-136. DOI:10.1021/jp1080687

27. Kuznetsov VL, Butenko YV. Nanodiamond graphitization and properties of onion-like carbon. *NATO Science Series II: Mathematics, Physics and Chemistry*. 2005;192:199-216. DOI:10.1007/1-4020-3322-2_15

28. Zhang P, Wang J, Wang L, Li J, et al. Dense tungsten carbide bulks by self-densification reaction sintering of nanodiamond with tungsten at 1700 °C. *Ceramics International*. 2023;49(6):9287-9297. DOI:10.1016/j.ceramint.2022.11.095

29. Kvashnin AG, Rybkovskiy DV, Filonenko VP, Bugakov VI, et al. WB_{5-x}: synthesis, properties, and crystal structure – new insights into the long-debated compound. *Advanced Science*. 2020;7(16):2000775. DOI:10.1002/|advs.202000775

30. Dolmatov VYu, Kiselev MN, Senyut' VT, Bazanov OV, et al. Development of lightweight, durable tungsten pseudo-alloys with aluminum and copper in the presence of nanodiamonds. *New materials and*

technologies: powder metallurgy, composite materials, protective coatings, welding: materials of the 16th International Scientific and Technical Conference (Minsk, May 22-24, 2024), National Academy of Sciences of Belarus. Minsk: Belarusskaya Nauka; 2024. p. 344-347. (In Russ.)

31. Peskova AS, Vinogradova TS, Farmakovskij BV, Ulin IV, et al. *Alloy on the basis of the "iron-aluminum-copper-tungsten carbide" system*. Russian Federation patent 2,434,077 C1. 20 November 2011. (In Russ.)

32. Mikheev GM, Puzyr' AP, Vanyukov VV, Purtov KV, et al. Nonlinear scattering of light in nanodiamond hydrosol. *Technical Physics Letters*. 2010;36(4):358-361. DOI:10.1134/S1063785010040206

33. Vanyukov VV, Mikheev GM, Mogileva TN, Puzyr AP, et al. Polarization-sensitive nonlinear light scattering and optical limiting in aqueous suspension of detonation nanodiamonds. *Journal of the Optical Society of America B*. 2014;31(12):2990. DOI:10.1364/JOSAB.31.002990

34. Mikheev GM, Mikheev KG, Mogileva TN, Puzyr AP, Bondar VS. Basic of images laser recording technology on the detonation nanodiamond films. *Himicheskaya fizika i mezoskopiya*. 2013;15(4):638-644. (In Russ.)

35. Mikheev GM, Mikheev KG, Mogileva TN, Puzyr AP, Bondar VS. Laser image recording on detonation nanodiamond films. *Quantum Electronics*. 2014;44(1):1-3. DOI:10.1070/QE2014v044n01ABEH015299

36. Vanyukov V, Mogileva T, Mikheev G, Puzir A, et al. Size effect on the optical limiting in suspensions of detonation nanodiamond clusters. *Applied Optics*. 2013;52(18):4123-4130. DOI:10.1364/AO.52.004123

37. Vanyukov VV, Mikheev GM, Mogileva TN, Puzyr AP, et al. Near-IR nonlinear optical filter for optical communication window. *Applied Optics*. 2015;54(11): 3290. DOI:10.1364/AO.54.003290

38. Muller O, Pichot V, Merlat L, Spitzer D. Optical limiting properties of surface functionalized nanodiamonds probed by the Z-scan method. *Scientific Reports*. 2019;9(1):519. DOI:10.1038/s41598-018-36838-7

39. Shilova OA, Hamova TV, Panova GG, Anikina LM. *Method for pre-sowing treatment of barley seeds*. Russian Federation patent 2,618,143 C1. 2 May 2017. (In Russ.)

40. Panova GG, Shilova OA, Hamova TV, Anikina LM, et al. The effect of nanocomposite silica shell on the surface of seeds on the initial stages of plant development. *Agrofizika*. 2017;2:30-39. (In Russ.)

41. Shilova OA, Panova GG, Hamova TV, Nikolaeva AM, et al. Selection and application of nanoparticles as biologically active additives in agricultural technologies. *In the collection of abstracts "The Second International Symposium Chemistry for Biology, Medicine, Ecology and Agriculture", Russian Federation, Saint Petersburg, December 6-8;* 2021. p. 30-31. (In Russ.)

42. Shilova O, Dolmatov V, Panova G, Khamova T, et al. Nanodiamond batch enriched with boron: properties and prospects for use in agriculture. *Biointerface Research in Applied Chemistry*. 2022;12(5):6134-6147. DOI:10.33263/BRIAC125.61346147

43. Mishin AA, Krushenko GG. Plastic lubricants containing nanodiamond powders. *Aktual'nyye problemy aviatsii i kosmonavtiki*. 2012;1(8):122-123. (In Russ.)

44. Nusinov MD. *Space vacuum and the reliability of space technology*. Moscow: Znanie; 1986. 63 p. (In Russ.)

45. Shchelkanov SI, Red'kin VE, Dokshanin SG, Terent'ev VF, Lyamkin AI. *Plastic grease*. Russian Federation patent 2,163,921 C. 10 March 2001. (In Russ.)

46. Artymuk TN, Potapov VM. The use of nanodiamonds in increasing the life of the ICE. The state and innovations of technical service of machinery and equipment. *Proceedings of the VIII Regional Scientific and practical Conference of students and postgraduates, 10-11 November, Novosibirsk, Russian Federation.* Novosibirsk: Zolotoy kolos; 2016. p. 93-95. (In Russ.)

47. Novakov IA, Rahimova NA, Krasnov AP, Zheltobryuhov VF, et al. Features of using nanocomposites Na^+ – montmorillonite – polyfluorinated alcohol as an antifriction solid lubricant. *Izvestiya Volgogradskogo gosudarstvennogo tehnicheskogo universiteta*. 2012;5(92):174-178. (In Russ.)

48. Rahimova NA, Kudashev SV. Hydrophobization of bentonite with polyfluorinated alcohols. *Izvestiya Volgogradskogo gosudarstvennogo tehnicheskogo universiteta*. 2010;2(62):49-53. (In Russ.)

49. Musaeva RA. *On the interaction of nanoscale particles with lubricants in ICE.* Available from: https://science-bsea.narod.ru/2011/mol_2011/musaeva_vz.htm [Accessed 15 January 2026]. (In Russ.)

50. Vereshchagin AL. *Properties of detonation nanodiamonds*. Biysk: Altai State Technical University Publ. House; 2005. 134 p. (In Russ.)

51. Naryzhnyj SYu, Dolmatov VYu, Kozlov AS, Fomenko VV, et al. Influence of modified carbon allotropes on the combustion process of model composite rocket fuels. *In: All-Russian conference 'Physics of explosion: theory, experiment, applications', September 18-21, 2023, Novosibirsk, Russia.* Novosibirsk: Sibirskoye otdeleniye Rossiyskoy akademii nauk; 2023. p. 88. DOI: 10.53954/9785604990025_88 (In Russ.)

Information about the authors / Информация об авторах

Valerii Yu. Dolmatov, D. Sc. (Eng.), Head of research laboratory, Special Construction and Technology Bureau "Technolog", St. Petersburg, Russian Federation; ORCID 0000-0001-8643-0404; e-mail: diamondcentre@mail.ru

Долматов Валерий Юрьевич, доктор технических наук, начальник научно-исследовательской лаборатории, Специальное конструкторско-технологическое бюро «Технолог», Санкт-Петербург, Российская Федерация; ORCID 0000-0001-8643-0404; e-mail: diamondcentre@mail.ru

Alexander A. Merkin, D. Sc. (Eng.), Director-Chief Designer, Special Construction and Technology Bureau "Technolog", St. Petersburg, Russian Federation; e-mail: merkin@sktb-technolog.ru

Maxim N. Kiselev, General Director, JSC "Plant "Selmash", Kirov, Russian Federation; e-mail: maksimel1977-77@mail.ru

Nataliya P. Satonkina, D. Sc. (Phys. and Math.), Senior Researcher, Lavrentiev Institute of Hydrodynamics, Siberian Branch of RAS, Novosibirsk; Russian Federation; ORCID 0000-0002-5894-7497; e-mail: n.satonkina@g.nsu.ru

Natalia M. Lapchuk, Cand. Sc. (Phys. and Math.), Associate Professor, Belarusian State University, Minsk, Belarus; Scopus ID 6506141523; e-mail: lapchuk@bsu.by

Anna N. Oleshkevich, Engineer of the first category, Belarusian State University, Minsk, Belarus; e-mail: oleshkevich@bsu.by

Kristina V. Lotnikova, Research Engineer, Special Construction and Technology Bureau "Technolog", St. Petersburg, Russian Federation; ORCID 0009-0008-3331-4272; e-mail: lotnikova.k@bk.ru

Vladimir T. Senyut, Cand. Sc. (Eng.), Leading Researcher, The Joint Institute of Mechanical Engineering of the NAS of Belarus, Minsk, Belarus; ORCID 0000-0002-1595-8516; e-mail: vsenyut@tut.by

Sergey D. Pisarevsky, Cand. Sc. (Eng.), Chief Researcher, Geoinformation Systems of the NAS of Belarus, Minsk, Belarus; e-mail: pi_sar@mail.ru

Alla V. Nozhkina, D. Sc. (Chem.), Scientific Supervisor, JSC "Research Institute of Natural, Synthetic Diamonds and Tools", Moscow, Russian Federation; ORCID 0000-0003-4750-2625; e-mail: nojkina@inbox.ru

Alexander P. Ershov, D. Sc. (Phys. and Math.), Senior Researcher, Lavrentiev Institute of Hydrodynamics, Siberian Branch of RAS, Novosibirsk, Russian Federation; ORCID 0000-0003-2306-1837; e-mail: ers@hydro.nsc.ru

Меркин Александр Александрович, доктор технических наук, директор-главный конструктор, Специальное конструкторско-технологическое бюро «Технолог», Санкт-Петербург, Российская Федерация; e-mail: merkin@sktb-technolog.ru

Киселев Максим Николаевич, генеральный директор, АО «Завод «Сельмаш», Киров, Российская Федерация; e-mail: maksimel1977-77@mail.ru

Сатонкина Наталья Петровна, доктор физико-математических наук, ведущий научный сотрудник, Институт гидродинамики им. М. А. Лаврентьева СО РАН, Новосибирск, Российская Федерация; ORCID 0000-0002-5894-7497; e-mail: n.satonkina@g.nsu.ru

Лапчук Наталья Михайловна, кандидат физико-математических наук, доцент, Белорусский государственный университет, Минск, Республика Беларусь; Scopus ID 6506141523; e-mail: lapchuk@bsu.by

Олешкевич Анна Николаевна, инженер первой категории, Белорусский государственный университет, Минск, Беларусь; e-mail: oleshkevich@bsu.by

Лотникова Кристина Витальевна, инженер-исследователь третьей категории, Специальное конструкторско-технологическое бюро «Технолог», Санкт-Петербург, Российская Федерация; ORCID 0009-0008-3331-4272; e-mail: lotnikova.k@bk.ru

Сенють Владимир Тадеушевич, кандидат технических наук, ведущий научный сотрудник, Объединенный институт машиностроения НАН Беларуси, Минск, Республика Беларусь; ORCID 0000-0002-1595-8516; e-mail: vsenyut@tut.by

Писаревский Сергей Дмитриевич, кандидат технических наук, главный научный сотрудник, УП «Геоинформационные системы» НАН Беларуси, Минск, Республика Беларусь; e-mail: pi_sar@mail.ru

Ножкина Алла Викторовна, доктор химических наук, научный руководитель, ОАО «Научно-исследовательский институт природных, синтетических алмазов и инструмента», Москва, Российская Федерация; ORCID 0000-0003-4750-2625; e-mail: nojkina@inbox.ru

Ершов Александр Петрович, доктор физико-математических наук, главный научный сотрудник, Институт гидродинамики имени М. А. Лаврентьева СО РАН, Новосибирск, Российская Федерация; ORCID 0000-0003-2306-1837; e-mail: ers@hydro.nsc.ru

Received 15 January 2026; Revised 24 February 2026; Accepted 27 February 2026